Lithos 105 (2008) 118–128

Contents lists available at ScienceDirect

Lithos

journal homepage: www.elsevier.com/locate/lithos

U–Pb zircon age, geochemical and isotopic characteristics of carbonatite and syenite complexes from the Shaxiongdong, China

Cheng Xu [a,*], Ian H. Campbell [b], Charlotte M. Allen [b], Yanjing Chen [c], Zhilong Huang [a], Liang Qi [a], Guishan Zhang [a], Zaifei Yan [a]

[a] Laboratory of Materials of the Earth's Interior and Geofluid Processes, Institute of Geochemistry, Chinese Academy of Sciences, Guiyang 550002, China
[b] Research School of Earth Sciences, Australian National University, Canberra, Australia
[c] Department of Geology, Peking University, Beijing 100871, China

ARTICLE INFO

Article history:
Received 23 June 2007
Accepted 1 March 2008
Available online 18 March 2008

Keywords:
South Qinling
South China block
Carbonatite and syenite complexes
Calcite cumulates
Rifting environment
Plume

ABSTRACT

The Qinling is an important orogenic belt, which formed by the joining of the North China and South China blocks. The Shaxiongdong carbonatite–syenite complexes were emplaced at the southern margin of South Qinling and border the South China block. LA-ICPMS (Laser Ablation Inductively Coupled Plasma Mass Spectrometry) zircon U–Pb geochronology constrains the syenite emplacement age to be 441.8±2.2 Ma, which is significantly earlier than the collision of the South China block and South Qinling along the Mianlue suture (200–240 Ma) near where the complexes reside. Trace-element abundances and C–O–Sr–Nd–Pb isotopes for the carbonatites and calcite separates indicate an igneous origin. They and associated syenites show overlaps of initial $^{87}Sr/^{86}Sr$ ratios (0.7029–0.7033, 0.7030–0.7032) and ε_{Nd} (2.8 to 4, 2.5 to 6 for syenites and carbonatites, respectively), which implies that the carbonatites may derive from a carbonated alkali silicate melt. However, the rocks are composed dominantly of calcite. They have markedly lower Th, Nb, Zr and P contents compared to average calciocarbonatites worldwide. Calcites from the carbonatites are also characterized by low REE contents and relatively flat REE patterns. This indicates that the carbonatites are calcite-rich cumulates, which were produced from a residual liquid derived from an intensively fractioned carbonatite magma. In addition, the syenites are characterized by negative Pb and no Nb anomalies. They show lower Sr isotopes and higher ε_{Nd} than syn/post-orogen related granites emplaced in the Qinling. This indicates that the complexes formed in a rifting environment. It is noted that Sr and Nd isotopic compositions from the carbonatites and syenites are close to HIMU mantle source values. Variations in $^{207}Pb/^{206}Pb$ (0.785–0.842) and $^{208}Pb/^{206}Pb$ (1.954–2.110) ratios from the calcites best fit a model involving mixing HIMU and EM1 components. Therefore, plume activity may play an important role in the complex generation and tectonic evolution of the South China block. Geological support for this deduction is the presence of numbers of Silurian dyke swarms. We hypothesize that the upwelling plume metasomatizing the continental lithosphere resulted in the South Qinling separating from South China block along the Mianlue suture during the early Paleozoic period.

1. Introduction

Carbonatites are mantle-derived magmatic rocks commonly occurring within rift settings and associated with alkaline rocks. This rock type can provide valuable information on the compositions of the mantle because: (1) their isotopic ratios are inherited from the mantle source, aided by very high Sr and Nd concentrations (Bell and Blenkinsop, 1987; Nelson et al., 1988); (2) they have low viscosities (Treiman, 1989) which ensure rapid ascent to the surface (Williams et al., 1986). The petrogenesis of carbonatites worldwide, however, remains controversial. There are several principal hypotheses: (1) direct melting of a carbonate-bearing mantle source (e.g. Sweeney, 1994; Harmer and Gitiins, 1998; Srivastava et al., 2005), (2) generation as immiscible liquids from a CO_2-rich silicate magmas (e.g. Koster van Groos and Wyllie, 1963; Kjarsgaard and Hamilton, 1989; Halama et al., 2005), (3) products of extensive crystal fractionation from a CO_2-rich silicate magma (e.g. Lee and Wyllie, 1994; Veksler et al., 1998a). Note that because calcite crystals can float rapidly and separate from their low viscosity host carbonate magma (Wyllie and Tuttle, 1960), some researchers suggest that most calciocarbonatites are cumulates (e.g. Ionov and Harmer, 2002; Xu et al., 2007).

* Corresponding author. Institute of Geochemistry, Chinese Academy of Sciences, 46 Guanshui Road, Guiyang 550002, Guizhou Province, China. Tel.: +86 851 5895194; fax: +86 851 5891117.
E-mail address: xucheng1999@hotmail.com (C. Xu).

0024-4937/$ – see front matter © 2008 Elsevier B.V. All rights reserved.
doi:10.1016/j.lithos.2008.03.002

The Shaxiongdong carbonatite–syenite complexes are located on the southern rim of the Qinling orogenic belt and adjacent the South China block. The Qinling lies in central China striking east–west for more than 100 km. It is the contact zone between the North China and South China blocks, and ties into the Kunlun and Qilian orogens to west (Fig. 1). They together make a sizeable tectonic zone in East Asia. The orogenic belt has been well investigated, and a number of models have been advanced (e.g., Mattauer et al., 1985; Xue et al., 1996; Meng and Zhang, 2000; Ratschbacher et al., 2003). It is accepted that there are discrete sutures of different ages marking collision boundaries between the South China block, Qinling and North China block. The middle Paleozoic collision along the Shangdan suture accreted only the South Qinling to the southern part of North China block (including North Qinling). The late Triassic collision of the South China block with South Qinling along the Mianlue suture led to final integration of the North China and South China blocks (Fig. 1). It is important to note that this appears to be an amalgamation of the South Qinling and South China blocks as they appear to have been a single unit before Sinian (~800 Ma) (Lu et al., 2006). The tectonic settings are unknown. The zircon U–Pb age obtained in this study shows that the Shaxiongdong syenites were emplaced in early Paleozoic. Thus, studies on the Shaxiongdong carbonatites and associated syenites can potentially provide information about the mantle that underlaid this critical region. Presently, little geochemical work has been carried out on the complexes except the study of Li (1991). In this paper Laser Ablation Inductively Coupled Plasma Mass Spectrometry (LA-ICPMS) was used to date zircon from the syenite. Additionally, we report major and trace-element chemistry and C–O–Sr–Nd isotopic data for the Shaxiongdong carbonatites and syenites. Trace element and Pb isotopic data of carbonate minerals from the carbonatites in thin sections were determined by in-situ LA-ICPMS. Our objectives are to understand the petrogenesis, source characteristics, and tectonic constraints on generating carbonatite and syenite magmas of Shaxiongdong.

2. Geological setting

Tectonically, the Qinling orogenic belt is divided into two parts, North Qinling and South Qinling, separated by the Shangdan suture (Fig. 1). The northern border of the North Qinling is marked by a relatively narrow, straight and steep north-dipping fault zone, the Machaoying fault zone, which is a normal fault associated with the Cenozoic rifting basin to the north. The southern border of the South Qinling which separates it from the South China block is the Mianlue suture, which is greatly modified by late Mesozoic thrusting. The Qinling Precambrian basement is divided into two types (Meng and Zhang, 2000; Li et al., 2003): (1) late Archean to Paleoproterozoic crystalline basement, and (2) Mesoproterozoic to Neoproterozoic supracrustal basement. The crystalline basement is composed largely of amphibolite and granulite facies assemblages, as represented by the Qinling and Douling groups. The supracrustal basement consists of low-grade metamorphic rock assemblages, as represented by the Kuanping, Wudang and Yaolinghe groups. Sedimentologically, the North Qinling and South Qinling show different stratigraphic-sedimentary sequences from late Neoproterozoic to early Triassic (see Fig. 4 in Meng and Zhang, 2000). The Qinling is interpreted as a multi-system orogenic belt with two mountain chains associated with Shangdan and Mianlue sutures. The North Qinling is regarded as a middle Paleozoic orogen along the Shangdan suture with widespread Paleozoic

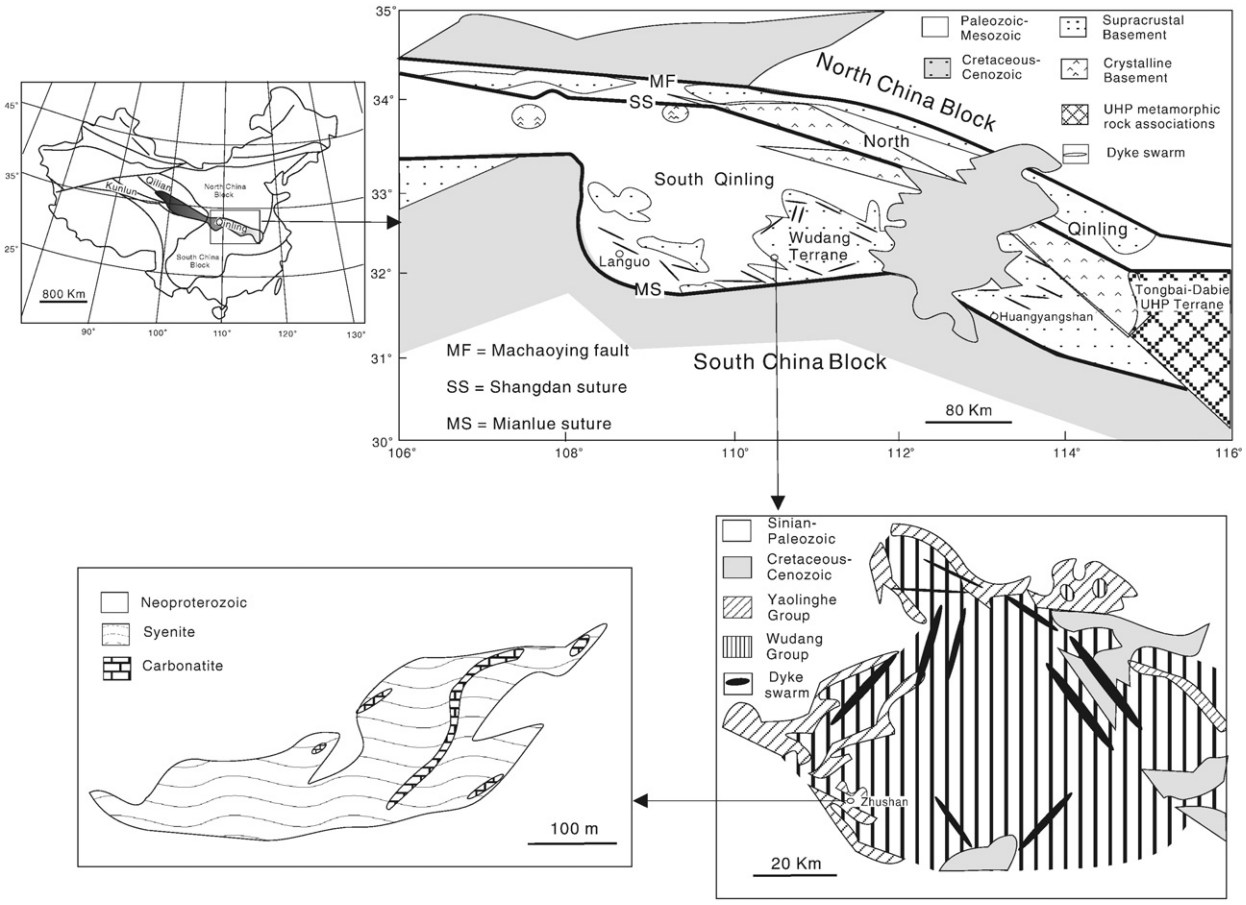

Fig. 1. Geological sketch of the Shaxiongdong carbonatites and syenites (modified after Li, 1991; Xue et al., 1996; Lu et al., 2006).

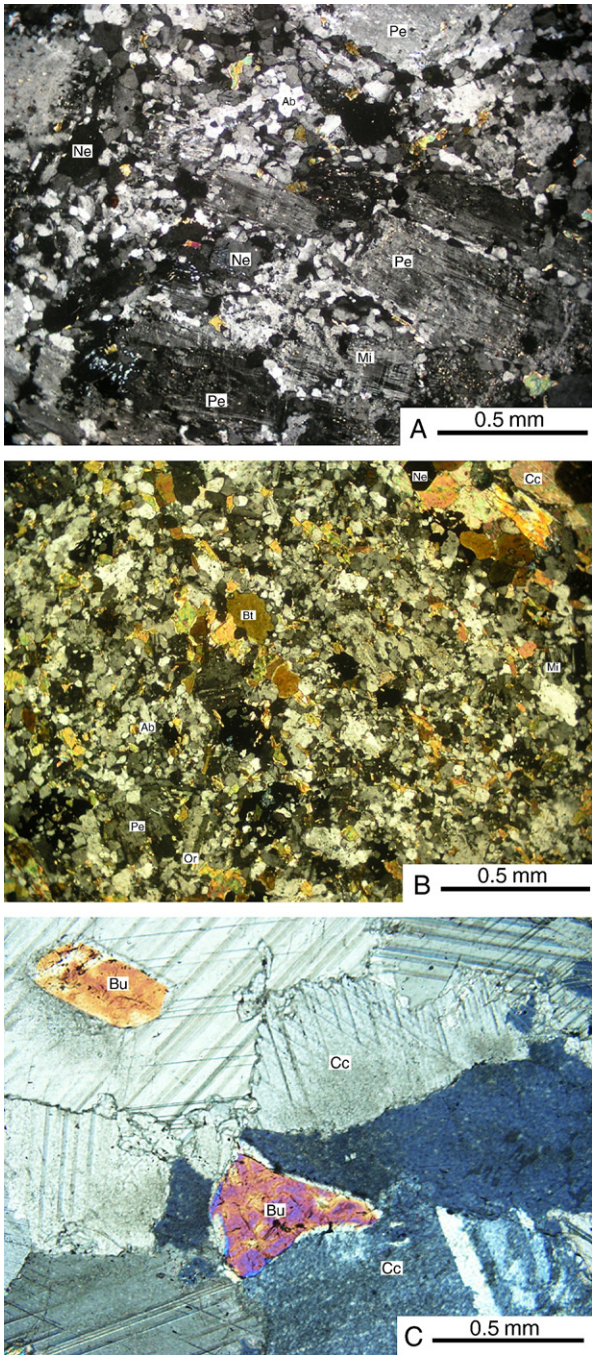

Fig. 2. Photomicrographs of the Shaxiongdong carbonatites and syenites (plane-polarized transmitted light). (A) Porphyritic syenite; (B) fine-grained syenite; (C) carbonatite. Pe, perthite; Mi, microcline; Or, orthoclase; Ab, albite; Ne, nepheline; Bt, biotite; Cc, calcite; Bu, burbankite.

island-arc type magmatism and metamorphism (Sun et al., 2002). The South Qinling is interpreted as a late Paleozoic to early Mesozoic orogen along the Mianlue suture with abundant Triassic granites and metamorphism (Mattauer et al., 1985; Sun et al., 2000). Consensus from the literature is that the North Qinling was an active continental margin, whereas the South Qinling was a passive margin and constituted the northernmost portion of the South China block (Lu et al., 2006).

The Shaxiongdong carbonatite and syenite complexes are located in the southwestern margin of Wudang Terrane, which is composed of Wudang and Yaolinghe groups (Fig. 1). The Wudang group is composed of alkaline basalt, keratophyre, quartz-keratophyre, dacite, rhyolite and pyroclastic rocks. The Yaolinghe group consists of tholeiite, spilitic diabase, spilite and keratophyre as well as interbedded clastics (Huang, 1993). These rocks underwent greenschist facies metamorphism. The complexes crosscut in the Yaolinghe group, and trend ENE to WSW. The syenites are composed mainly of K-feldspar and albite, with minor amounts of biotite, nepheline, aegirine and chlorite, and accessory minerals such as muscovite, calcite, barite, apatite, epidote, pyrochlore, titanite, magnetite, ilmenite, burbankite, zircon and sulfides. The K-feldspar mainly includes perthite, microcline and orthoclase. This rock is a nepheline-bearing alkali-feldspar syenite (Le Maitre et al., 1989). They are generally K-feldspar porphyritic and the proportion of phenocrysts is high although there are some fine-grained rocks (Fig. 2A, B). The latter occur at contacts with the carbonatites and is altered and impregnated by calcite (Fig. 2B). The carbonatites intrude syenites as dykes with length of tens to more than 200 m. They are composed of calcite (>80%), with individual crystal generally >0.1 mm in size. Minor and accessory phases include K-feldspar, albite, aegirine, biotite and burbankite, apatite, barite, pyrochlore, magnetite, ilmenite, perovskite, allanite, zircon and sulfides. REE minerals occur mostly as burbankite and allanite which make up 1–2% of the rock by volume (Wang and Yan, 1989; Fig. 2C). Monazite and bastnäsite are absent in the carbonatites.

3. Analytical methods

U–Th–Pb age determination of zircons in syenite was analyzed by Agilent HP7500S LA-ICPMS at the Australian National University. The zircons in syenite were separated using conventional magnetic and heavy liquid separation techniques, then mounted in epoxy resin and polished. Optical photomicrographs were used to map and select least-fractured and inclusion free material for analysis. Dating by LA-ICPMS has been described by Campbell et al. (2005). In this case, the resulting ratios were concordant within analytical uncertainties where we used agreement of $^{206}Pb/^{238}U$ and $^{207}Pb/^{235}U$ ages as a measure of concordancy. Uncertainties reported on individual grains were a combination of measured uncertainty in the $^{206}Pb/^{238}U$ age for the individual analysis and the uncertainty on the average Temora $^{206}Pb/^{238}U$ (0.5% here). 98-521, an in-house standard thought to be 42.6 Ma in age (n=340 in 22 analytical sessions) was treated as an unknown, and on this day gave 42.4±0.2 with MSWD of 0.52 confirming that dates are accurate, and that our estimates of uncertainty in the measurements are appropriate or perhaps generous. SHRIMP analyses of 98-521 gave 43.1±0.6 for 10 spots in one analytical session (Ballard et al., 2001). Cathodoluminescence (CL) images were obtained using a Quanta400 FEG scanning electron microscope at the Northwest University in Xi'an. It was operated at an accelerating voltage of 10 kV, a beam current of 8 nA and a working distance of 8 mm. CL images reveal the internal patterns of the zircons, thus providing useful information on the formation history of the crystals.

Major elements of whole rock samples were determined by wet chemical methods at the Institute of Geochemistry, Chinese Academy of Sciences. Major element compositions of carbonate minerals were measured on C-coated polished section by

Table 1
Representative EPMA data for carbonate minerals in carbonatites

Samples	SXD-1-1	SXD-1-2	SXD-1-3	SXD-2-1	SXD-2-2	SXD-2-3	SXD-4-1	SXD-4-2	SXD-8-1	SXD-8-2
MgO	0.66	0.59	0.64	1.09	1.07	1.27	0.73	0.83	0.40	0.45
CaO	51.88	51.08	50.31	49.21	50.47	46.27	47.76	47.55	50.53	48.16
MnO	2.72	2.50	2.74	2.64	2.38	2.63	2.90	2.77	2.50	2.70
FeO	2.59	2.12	2.41	2.69	2.94	2.63	2.54	2.82	1.59	1.78
SrO	4.64	4.10	4.24	3.65	3.76	6.54	3.94	3.66	4.10	2.29

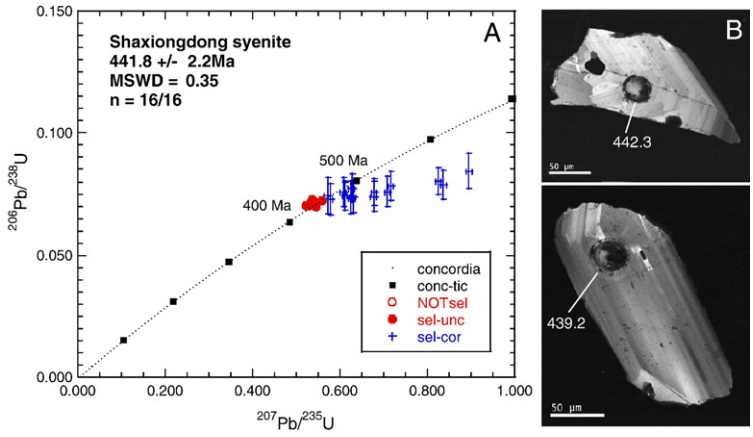

Fig. 3. Concordia plots (A) of LA-ICPMS U–Pb results used in calculating the zircon age of syenite and cathodoluminescence images (B) of the zircons with laser pits and corresponding U–Pd ages. In A ticks represent 100 million year intervals (conc-tic). The uncorrected data are circles (NOTsel), where the filled equals the selected data used for the final age calculation (sel-unc). The crosses are data both ^{208}Pb and ^{230}Th corrected with 2σ uncertainties including uncertainties in standards (sel-cor).

wavelength-dispersive EPMA-1600 electron microprobe at the Institute of Geochemistry, Chinese Academy of Sciences using an accelerating voltage of 25 kV and a beam current of 10 nA. The beam was defocused to 10–20 μm spot size to limit devolatilization of the carbonates. Mineral standards used for calibration were calcite (Ca), dolomite (MgO), willemite (Mn), olivine (Fe) and celestine (Sr).

Table 2
Major and trace-element compositions of syenites and carbonatites

Samples	SXD-01	SXD-02	SXD-03	SXD-20	SXD-21	SXD-23	SXD-24	SXD-25	SXD-28	SXD-29	SXD-30	SXD-1	SXD-2	SXD-3	SXD-4	SXD-5	SXD-8
Type	FS	FS	FS	PS	PS	PS	PS	PS	PS	PS	PS	C	C	C	C	C	C
Major elements (wt.%)																	
SiO_2	50.09	50.78	49.41	52.87	51.5	55.55	54.84	53.73	52.98	53.51	53.4	8.64	13.71	6.75	5.27	5.19	15.48
TiO_2	1.89	3.12	3.13	3.12	3.56	3.26	3.02	2.76	2.81	3.26	3.18	0.17	0.24	0.16	0.12	0.10	0.34
Al_2O_3	18.57	19.49	18.96	20.66	21.88	22.31	21.06	21.27	21.57	20.95	20.74	3.56	10.55	5.78	6.25	10.75	14.21
FeO_t	8.74	10.07	8.86	4.89	4.61	4.03	3.84	4.38	5.0	4.62	4.64	3.95	6.10	2.48	3.04	5.06	4.85
MnO	0.17	0.28	0.20	0.07	0.16	0.07	0.18	0.23	0.28	0.07	0.07	1.0	1.57	0.23	1.11	0.61	1.35
MgO	0.81	1.94	1.48	0.53	0.29	0.16	0.46	0.31	0.40	0.20	0.18	0.74	1.86	0.46	0.40	0.79	0.60
CaO	5.33	1.67	5.5	2.05	2.06	0.53	0.79	0.93	1.21	1.75	2.04	45.56	35.18	47.04	46.29	42.44	31.17
Na_2O	7.48	5.77	4.58	7.74	4.94	8.65	8.42	11.0	7.31	7.62	7.82	0.48	1.91	0.2	0.28	0.32	1.72
K_2O	1.95	2.04	1.96	4.65	4.48	2.6	4.01	2.09	3.23	3.87	3.70	0.30	1.53	0.21	0.06	1.07	1.51
H_2O	4.42	4.17	5.37	2.81	5.72	2.75	3.13	3.15	4.44	3.79	3.54						
P_2O_5	0.28	0.32	0.28	0.32	0.52	0.26	0.15	0.23	0.38	0.45	0.47	0.12	0.14	0.25	0.07	0.30	0.28
CO_2												35.25	26.85	36.3	36.86	33.12	28.08
Total	99.73	99.65	99.73	99.71	99.72	100.17	99.90	100.08	99.61	100.09	99.78	99.77	99.64	99.86	99.75	99.75	99.59
Trace elements (ppm)																	
Rb	85.2	85.0	81.8	132	98.1	53.1	88.8	27.0	47.9	76.2	56.1	10.4	71.7	6.47	28.5	42.6	32.7
Ba	2441	785	878	6024	7108	1633	4538	2840	3955	3994	5645	3058	1736	4473	2812	2665	2774
Th	27.0	37.3	54.0	5.10	2.31	5.85	7.99	22.0	11.6	8.43	7.65	4.35	9.90	4.92	1.02	4.95	6.65
U	2.99	2.91	2.79	11.8	5.2	14.2	26.5	21.7	25.4	20.0	11.7	0.31	6.93	0.22	0.19	0.50	2.62
Nb	137	123	140	433	191	547	578	661	828	230	348	22.0	476	16.4	38.1	47.3	84.8
Ta	9.60	9.13	9.27	4.48	2.34	6.08	8.58	9.15	4.53	7.98	4.36	0.24	1.14	0.15	0.15	0.20	0.68
Pb	3.76	3.91	3.63	6.25	6.85	5.72	7.83	7.56	9.04	6.89	12.3	30.8	17.6	58.3	39.3	30.0	27.4
Sr	3964	2508	4262	1889	1638	1715	1521	2852	4567	1616	2091	23620	20000	33080	27400	24920	20390
Zr	402	595	415	244	93.0	273	792	1241	210	1543	630	2.85	17.5	2.52	1.02	2.06	90.1
Hf	8.30	13.6	8.48	3.17	1.35	4.37	7.75	13.6	2.96	14.3	6.30	0.26	0.45	0.22	0.19	0.19	1.33
Y	35.6	35.8	36.3	6.07	12.3	6.02	13.0	18.0	16.2	7.76	13.4	129	103	83.6	95.7	113	131
Ga	31.2	30.7	29.7	40.9	38.5	43.9	50.9	47.5	52.5	40.2	35.7	26.6	37.8	81.2	49.3	50.9	38.5
La	133	89.7	117	40.5	60.5	32.6	315	270	573	172	41.7	745	670	3432	1865	1665	1126
Ce	351	205	334	71.0	86.8	58.7	463	420	821	305	73.3	1291	1141	5688	3136	2647	1763
Pr	31.4	25.2	32.0	7.39	9.39	5.85	33.3	33.2	56.6	20.9	8.64	114	99	394	243	222	122
Nd	117	105	123	24.3	30.5	18.8	99.2	107	167	57.8	31.9	393	325	1126	646	592	454
Sm	18.8	19.0	20.5	3.36	4.72	2.71	10.1	13.5	16.1	6.06	5.96	55.7	45.9	87.46	76.1	67.6	55.3
Eu	5.44	5.59	5.86	0.87	1.39	0.75	2.41	3.55	3.78	1.41	1.59	15.5	13.8	21.9	19.2	18.1	16.8
Gd	15.3	18.4	15.7	2.99	4.59	2.27	9.91	12.4	16.6	6.12	5.0	49.7	47.2	109.8	71.5	62.6	66.9
Tb	1.76	1.90	1.88	0.31	0.53	0.25	0.80	1.19	1.27	0.46	0.65	6.58	5.23	8.21	7.02	6.39	6.59
Dy	8.12	8.50	8.50	1.39	2.60	1.13	3.06	4.74	4.34	1.75	3.35	31.5	23.2	27.4	28.0	29.1	30.3
Ho	1.44	1.44	1.46	0.25	0.44	0.23	0.52	0.76	0.71	0.32	0.60	5.81	4.10	4.53	4.77	5.27	5.01
Er	3.72	4.07	3.87	0.69	1.14	0.74	1.55	1.98	2.04	1.04	1.58	15.5	10.7	12.7	14.5	14.8	13.3
Tm	0.47	0.47	0.47	0.09	0.14	0.11	0.18	0.23	0.22	0.15	0.22	1.81	1.38	1.37	1.65	1.78	1.70
Yb	2.81	2.90	2.85	0.60	0.86	0.69	1.15	1.43	1.32	1.05	1.47	9.70	7.51	7.35	8.16	9.57	9.77
Lu	0.40	0.42	0.40	0.09	0.12	0.10	0.17	0.19	0.18	0.16	0.21	1.49	1.10	1.13	1.20	1.33	1.48
La/Yb_N	31.8	20.8	27.7	45.5	47.4	31.8	184	127	293	110	19.2	52.2	60.6	317	155	118	78.3
Gd/Yb_N	4.39	5.11	4.46	4.03	4.30	2.65	6.93	6.96	10.1	4.70	2.75	4.15	5.08	12.1	7.09	5.29	5.54

FS, fine-grained syenite; PS, porphyritic syenite; C, carbonatite; FeO_t, total Fe calculated as FeO; N, normalized by chondrite.

Table 3
LA-ICPMS analyses of calcite crystals

Samples	SXD-1-1		SXD-1-2		SXD-1-3		SXD-1-4		SXD-1-5		SXD-1-6	SXD-2-1	SXD-2-2	SXD-2-3	SXD-2-4	SXD-2-5	SXD-2-6	
	Rim–Core		Rim–Core		Rim–Core		Rim–Core		Rim–Core		Core	Core	Core	Core	Core	Core	Rim–Core	
Rb	0.06	0.05	bdl	0.08	0.05	0.07	0.06	0.11	0.05	0.04	bdl	bdl	bdl	bdl	bdl	bdl	bdl	bdl
Ba	436	569	336	439	448	468	605	474	379	483	588	581	614	568	626	620	512	555
Th	bdl	bdl	bdl	0.04	0.03	0.11	0.06	0.03	0.03	0.06	0.03	bdl	bdl	bdl	bdl	bdl	bdl	bdl
U	bdl	bdl	bdl	bdl	bdl	bdl	bdl	bdl	bdl	bdl	bdl	bdl	bdl	bdl	bdl	bdl	bdl	bdl
Nb	bdl	bdl	bdl	0.01	0.003	bdl	0.002	0.01	bdl	0.005	0.003	bdl	bdl	bdl	bdl	bdl	bdl	bdl
Ta	bdl	bdl	bdl	bdl	bdl	bdl	bdl	bdl	bdl	bdl	bdl	bdl	bdl	bdl	bdl	bdl	bdl	bdl
Pb	24.2	25.3	23.5	23.4	25.1	25.6	26.7	26.7	20.8	24.7	25.4	13.8	13.4	13.1	14.2	13.8	15.8	13.9
Sr	19304	20184	19594	20458	20314	20736	20967	21350	18848	22524	20573	16920	18318	17460	17575	17468	16966	16187
P	1.82	1.66	1.83	2.08	2.20	2.85	1.72	3.11	1.38	2.69	1.81	bdl	bdl	bdl	bdl	bdl	0.84	bdl
Zr	bdl	bdl	bdl	0.01	bdl	0.01	bdl	0.01	0.01	0.01	bdl	0.02	bdl	0.01	bdl	0.01	0.02	0.01
Ti	bdl	bdl	bdl	bdl	0.20	bdl	0.21	0.20	bdl	bdl	bdl	bdl	bdl	bdl	bdl	0.22	bdl	bdl
Y	144	158	159	134	215	167	176	102	153	141	151	112	116	106	107	105	53.5	70.7
Ga	38.1	48.5	28.1	35.6	36.1	37.0	46.7	36.9	30.1	37.7	45.0	81.3	84.2	76.8	82.5	80.5	66.1	70.6
La	53.1	62.6	49.7	97.0	77.5	131	85.0	104	49.0	132	68.0	38.1	37.7	28.2	37.7	32.7	22.2	20.0
Ce	157	183	145	254	237	352	237	271	142	350	193	105	111	81.8	105	92.8	54.8	50.1
Pr	22.5	26.0	20.5	32.9	34.4	45.7	32.6	34.3	19.6	44.2	26.6	14.7	15.9	11.7	14.5	13.1	6.89	6.3
Nd	111	126	102	148	172	209	156	151	96.1	195	127	67.9	75.1	54.2	67.1	61.5	27.7	25.9
Sm	33.3	37.3	34.0	35.6	52.0	50.0	44.0	34.2	28.4	45.6	35.8	20.8	23.0	17.6	20.1	18.8	6.88	7.6
Eu	11.4	12.7	12.4	11.5	17.9	16.0	14.9	10.6	9.9	14.1	12.3	8.0	8.7	6.8	7.6	7.0	2.40	3.0
Gd	33.5	37.3	36.9	32.9	52.9	45.1	43.0	28.7	29.6	38.5	35.4	23.7	25.7	21.0	22.4	21.9	6.39	9.3
Tb	5.50	6.11	6.21	5.29	8.54	6.95	6.96	4.41	5.08	5.76	5.77	4.25	4.50	3.86	3.93	3.77	1.29	1.94
Dy	32.8	35.5	36.3	31.1	49.0	40.0	39.6	24.5	32.0	32.3	33.2	25.2	26.4	23.4	23.4	22.9	9.19	13.1
Ho	5.94	6.43	6.60	5.70	8.94	7.23	7.16	4.32	6.15	5.81	6.09	4.86	5.03	4.51	4.37	4.38	2.09	2.80
Er	15.1	16.0	16.2	14.2	21.9	18.2	17.9	10.6	15.8	14.2	14.8	12.4	12.6	11.4	11.1	11.1	6.20	7.6
Yb	12.2	12.7	13.0	11.4	17.0	14.2	13.9	8.2	12.9	11.3	12.1	10.5	10.5	9.5	9.1	9.4	6.10	7.2
Lu	1.54	1.59	1.59	1.42	2.13	1.82	1.73	1.01	1.63	1.40	1.51	1.30	1.33	1.21	1.20	1.19	0.82	0.89
La/Yb_N	2.96	3.36	2.60	5.77	3.10	6.28	4.15	8.60	2.59	7.92	3.82	2.47	2.45	2.02	2.83	2.37	2.47	1.90
Gd/Yb_N	2.23	2.38	2.30	2.33	2.52	2.58	2.50	2.83	1.86	2.75	2.37	1.84	1.98	1.79	2.00	1.89	0.85	1.05
$^{207}Pb/^{206}Pb$	0.786	0.790	0.786	0.821	0.782	0.803	0.780	0.796	0.775	0.797	0.779	0.789	0.798	0.810	0.778	0.786	0.772	0.795
$^{208}Pb/^{206}Pb$	1.954	1.962	1.947	2.021	1.926	1.993	1.929	1.960	1.949	1.955	1.942	1.934	1.945	1.973	1.913	1.922	1.914	1.961

bdl, Below detection limits; N, normalized by chondrite. $^{207}Pb/^{206}Pb$ and $^{208}Pb/^{206}Pb$ are calculated that ratios between determined ^{207}Pb and ^{206}Pb, and ^{208}Pb and ^{206}Pb as calibration standard of NIST 610 multiplies 0.9098 and 2.169, respectively (Woodhead and Hergt, 2000). Pb concentrations in calcite crystal are modeled from ^{208}Pb.

The trace-element concentrations in carbonatites and syenites were analyzed by solution ICPMS (VG PQ-ExCell) at the University of Hong Kong. Method details are given by Liang et al. (2000). In-situ LA-ICPMS analyses of carbonate minerals in carbonatites in polished thin section were performed at the Australian National University. The diameter of the ablation spot varied between 54 and 86 μm. NIST 610 glass was used as a calibration standard for all carbonate samples. Calculation of element concentrations was like that reported by Eggins et al. (1997). The element used for the internal standard was Ca, measured as ^{43}Ca, expressed as CaO (mean; Table 1). Detection limits were calculated after Longerich et al. (1996). Analytical precision is ≤5% at the ppm level. In-run signal intensity for indicative trace elements was monitored during analysis to make sure that the laser beam stayed within the phase selected and did not penetrate inclusions. The LA-ICPMS results include Pb isotope ratios for masses 206, 207 and 208. Pb concentration is estimated from ^{208}Pb measurement. Isotope ratios are calculated directly from fractionation factors derived from analysis of the NIST glass standard. Note because of the presence of systemic Hg contamination measurement of ^{204}Pb was not possible.

The carbon and oxygen isotopic compositions of the carbonate minerals were measured at the Institute of Geochemistry, Chinese Academy of Sciences using continuous-flow isotope ratio mass spectrometer (IsoPrime). Analytical error is ±0.1‰ (1σ) for both carbon and oxygen, and the results are expressed conventionally as per mil (‰) variation relative to SMOW and PDB, respectively. For Sr isotopic analyses of carbonatites, fresh carbonate minerals were mounted in a polished epoxy mount with carbonate cores exposed. The analyses were performed with a Neptune LA-MC-ICPMS at the Australian National University. One to three carbonate grains from the same whole rock were repeatedly measured. The spot diameter used to measure these samples and standard was 178 and 233 μm, respectively. The average $^{87}Sr/^{86}Sr$ ratio obtained for the Tridacna standard was 0.70913, whose accepted value within laboratory is 0.70917. Syenite Sr, Nd and carbonatite Nd isotopic compositions were analyzed on a Finnigan MAT 262 mass spectrometer at the Institute of Geology and Geophysics, Chinese Academy of Sciences. Total procedural blanks were <100 pg for Sr and <50 pg for Nd. The mean $^{143}Nd/^{144}Nd$ ratios in the Ames standard was 0.512139±18 (2σ, n=28) during the course of this study. The value is fractionation corrected for a $^{146}Nd/^{144}Nd$ value of 0.7219. Fractionation effects during the Sr isotopic composition runs were eliminated by normalizing to a $^{86}Sr/^{88}Sr$ value of 0.1194. The mean $^{87}Sr/^{86}Sr$ ratio in the NBS987 standard was 0.710255±16 (2σ, n=33). The details for analytical processes of zircon U–Th–Pb age determination, trace elements and Sr–Nd isotopes of whole rocks are described online.

4. Results

4.1. U–Pb geochronology

Data from zircon samples analyzed by LA-ICPMS U–Pb geochronology are shown in Fig. 3 and Table A (online).

Zircons in syenite are short to long prismatic, and light pink. The lengths range from 150 to 300 μm. CL images of polished grains reveal clear oscillatory zoning, which is typical for magmatic zircon. Sixteen LA-ICPMS zircon U–Pb isotope analyses also yield relatively high Th/U ratios of 1.6 to 4.6 (Table A online), consistent with their igneous origin (Rubatto and Gebauer, 2000). These give a very tight, concordant result (Fig. 3) thus no common Pb correction was employed. They define a single, coherent population with a weighted mean $^{206}Pb/^{238}U$ age of 441.8±2.2 Ma (MSWD=0.35), which is interpreted as the emplacement age of the syenite.

Whole rock Sm–Nd and Rb–Sr ages from ophiolite complex rocks and zircon U–Pb ages from syncollisional granites in the Mianlue suture range from 221 to 242 Ma (Li et al., 1996) and 206 to 220 Ma (Sun et al., 2000), respectively. These ages constrain

SXD-3-1	SXD-3-2	SXD-3-3	SXD-3-4	SXD-3-5	SXD-4-1	SXD-4-2			SXD-4-3	SXD-4-4		SXD-8-1		SXD-8-2		SXD-8-3	SXD-8-4	SXD-8-5	SXD-8-6
Core	Core	Core	Core	Core	Core	Rim–Core			Core	Rim–Core		Rim–Core		Rim–Core		Core	Core	Core	Core
0.12	0.05	0.05	0.04	0.10	0.05	0.08	0.11	0.04	0.07	0.05	0.04	bdl	bdl	bdl	bdl	bdl	bdl	bdl	bdl
227	572	417	444	470	528	503	520	567	640	490	467	349	314	259	450	462	417	522	275
0.04	0.04	0.01	bdl	bdl	bdl	bdl	bdl	0.41	bdl	bdl	bdl	bdl	0.08	bdl	0.03	0.04	0.03	0.03	0.07
bdl	bdl	bdl	bdl	bdl	bdl	bdl	bdl	bdl	bdl	bdl	bdl	bdl	bdl	bdl	bdl	bdl	bdl	bdl	bdl
0.05	bdl	0.01	0.002	bdl	bdl	bdl	bdl	bdl	bdl	bdl	bdl	bdl	0.003	0.01	0.01	0.003	0.004	bdl	bdl
bdl	bdl	bdl	bdl	bdl	bdl	bdl	bdl	bdl	bdl	bdl	bdl	bdl	bdl	bdl	bdl	bdl	bdl	bdl	bdl
16.6	18.0	20.1	18.6	15.7	25.4	19.1	21.0	23.8	24.3	22.4	20.8	25.3	42.1	19.9	23.9	26.5	27.3	25.4	27.4
18215	16509	16719	15935	16262	18532	20715	18676	18250	16753	17695	18657	18151	19536	16705	18721	19152	18880	18591	18961
bdl	0.34	0.84	0.62	0.38	bdl	0.91	0.60	1.99	0.57	2.76	0.91	0.85	3.82	bdl	2.74	2.19	1.44	1.35	5.06
0.01	0.01	bdl	0.01	0.01	0.01	bdl	bdl	0.01	0.01	bdl	bdl	bdl	0.08	bdl	0.01	bdl	0.01	bdl	bdl
0.26	bdl	0.13	0.12	0.13	bdl	0.32	bdl	bdl	bdl	0.25	bdl	0.34	bdl	0.23	0.22	bdl	0.25	bdl	0.25
86.9	149	116	110	109	156	145	136	156	178	148	122	142	170	181	153	161	166	160	192
24.2	61.8	44.1	46.6	47.6	52.2	48.6	49.4	52.7	56.8	44.3	42.2	29.5	27.7	24.0	39.8	39.5	34.8	44.3	22.4
35.4	50.2	59.1	75.0	16.6	65.7	61.4	70.4	75.2	47.2	52.7	72.4	46.3	150	32.2	73.2	93.0	77.4	78.0	136
71.5	127	139	186	50.7	171	126	178	184	126	141	183	136	362	96.1	195	249	210	213	351
8.7	17.5	18.5	22.4	7.7	23.0	19.6	24.2	24.4	17.5	19.5	24.0	19.3	43.6	14.3	26.2	32.9	28.3	28.7	43.9
38.1	83.5	81.0	98.9	39.2	105.6	91.2	108	109	80.8	90.4	105	94.0	190	72.7	123	149	134	134	196
11.0	25.7	22.0	25.0	14.9	31.5	27.7	31.2	32.8	28.0	28.8	29.5	28.4	43.2	27.6	34.4	39.3	37.5	36.8	47.0
4.2	9.2	7.6	8.2	5.8	11.9	10.4	11.3	12.1	10.9	10.8	10.2	10.2	13.9	10.4	11.6	13.3	12.8	12.6	15.0
14.3	29.0	23.1	24.3	19.3	34.4	31.9	32.1	35.3	33.8	31.8	28.5	31.0	39.2	33.6	34.1	38.0	37.5	36.2	43.9
2.72	4.96	4.05	4.04	3.66	6.01	5.57	5.40	6.15	6.38	5.53	4.82	5.32	6.33	6.32	5.66	6.17	6.20	6.02	6.88
18.4	31.7	25.9	25.4	24.3	35.1	33.1	31.3	35.1	38.0	32.1	27.6	30.7	36.6	37.8	32.8	35.0	35.9	34.9	40.7
3.54	5.67	4.71	4.43	4.33	6.38	6.09	5.68	6.35	7.10	5.87	4.96	5.69	6.56	7.04	5.92	6.37	6.64	6.31	7.58
9.6	15.0	12.3	11.4	11.3	15.6	15.0	13.9	15.5	17.9	14.4	12.0	14.0	16.7	17.8	14.7	15.4	16.4	15.8	19.0
7.9	11.9	9.8	9.1	8.9	12.6	12.4	11.2	12.7	14.5	11.9	9.9	11.7	14.0	14.6	12.2	12.6	13.2	12.5	15.0
0.91	1.42	1.17	1.09	1.06	1.56	1.62	1.45	1.59	1.82	1.50	1.28	1.42	1.78	1.77	1.55	1.64	1.71	1.56	1.98
3.05	2.88	4.10	5.59	1.27	3.53	3.37	4.25	4.03	2.21	3.0	4.99	2.70	7.29	1.50	4.07	5.0	3.99	4.24	6.16
1.46	1.98	1.90	2.16	1.75	2.20	2.09	2.31	2.25	1.88	2.16	2.34	2.15	2.27	1.86	2.26	2.43	2.30	2.34	2.36
0.834	0.862	0.841	0.823	0.849	0.821	0.818	0.791	0.806	0.827	0.830	0.820	0.798	0.821	0.780	0.768	0.775	0.782	0.783	0.773
2.139	2.137	2.085	2.042	2.153	2.057	2.007	1.943	2.032	2.020	2.049	2.005	1.971	2.007	1.967	1.918	1.945	1.923	1.939	1.960

the collision between the South China block and South Qinling along the Mianlue suture to be Triassic. It is clear that the time of Shaxiongdong syenite formation is obviously earlier than the collisional event.

4.2. Element geochemistry

Concentrations of major and trace elements of carbonate minerals, carbonatites and syenites are summarized in Tables 1, 2 and 3.

The carbonate mineral from the carbonatites is typical calcite, with high CaO, Sr, and low MgO contents (Table 1). Their corresponding whole rocks have low SiO_2 (<15), FeO_t (<6), MgO (<2) and alkalis, with variable CaO/(CaO+MgO+FeO_t+MnO) ratios of 79–95%, and are calciocarbonatites (Woolley and Kempe, 1989).

The carbonatites are enriched in every element except for Zr, Hf and Ti on the primary mantle-normalized abundance diagrams (Fig. 4A). They show peaks for Ba, Nb, La, Sr, Nd, Eu and Gd. It is noted that the rocks are characterized by markedly lower Th, Nb, P and Zr contents relative to average calciocarbonatite worldwide. Chondrite-normalized REE patterns for the carbonatites are LREE enriched with high La/Yb_N ratios (52–317) and negligible Ce and Eu anomalies (Fig. 5A–E). The calcites contain somewhat lower abundances than their corresponding whole rocks except for Pb, Sr, Y and HREE. Some Th, U, Nb, Ta and Zr contents of the calcites are below detection limits (<ppm) of the LA-ICPMS. These elements are concentrated in accessory oxides, such as ilmenite-, perovskite-, pyrochlore-group phases and zircon (e.g. Chakhmouradian, 2006). In addition, the calcite cores generally have higher Sr, Pb and LREE compositions than rims (Table 3). They have very low REE abundances ranging from 70–600 times the chondritic value for La to 50–100 times the chondritic value for Yb, and relatively flat distribution patterns (Fig. 5A–E). The bulk of HREE resides in calcite whereas the LREE, enriched in the whole rock compared to calcite must reside in accessory phases. Non-carbonate minerals apatite, pyrochlore and perovskite are possible REE-rich phases, but their contents in bulk rocks are lower than 1% and cannot host the balance. The REE mineral burbankite is a possible host.

The nepheline-bearing alkali-feldspar syenites in general share the following features: (1) high K_2O+Na_2O contents and Na_2O/K_2O ratios (~2); (2) all samples are enriched in every element in Fig. 4C, and possess positive Ba (except for SXD-02, -03) and Sr and negative Pb (except for SXD-30) and P anomalies compared with the neighboring elements; (3) LREE enrichment relative to HREE with steep slopes (La/Yb_N=19–293) and slightly negative Eu anomalies (Fig. 5F). In addition, the porphyritic syenite has higher SiO_2, Al_2O_3, K_2O+Na_2O and lower FeO and MgO compositions than fine-grained syenite (Table 2). The former has greater LREE/HREE ratio (Fig. 5F). This variable REE distribution pattern is also found in nepheline syenite from northeastern India (Srivastava and Sinha, 2004).

4.3. C–O and Sr–Nd–Pb isotopic data

Carbon, oxygen, strontium, neodymium and lead isotopic data are given in Tables 3 and 4. The carbon isotopic compositions of five calcite separates from their corresponding carbonatites lie within a narrow range between −5.71 and −6.08‰ $\delta^{13}C$, and the oxygen isotopic compositions vary slightly from 6.92 to 8.09‰ $\delta^{18}O$, which are compatible with a primary magmatic, mantle-derived carbonatite (Fig. 6), i.e. unaffected by superficial secondary processes.

In-situ Sr isotopic analyses of calcites in carbonatites on average are low and range from 0.7030 to 0.7032, which are similar to the result reported by Li (1991) for a carbonatite sample (0.7032). High Sr contents and low Rb/Sr ratios of the calcites (Table 3) make it likely that the $^{87}Sr/^{86}Sr$ ratios of the calcites accurately reflect the composition of the carbonatite magma, which, in turn, reflect the composition of the

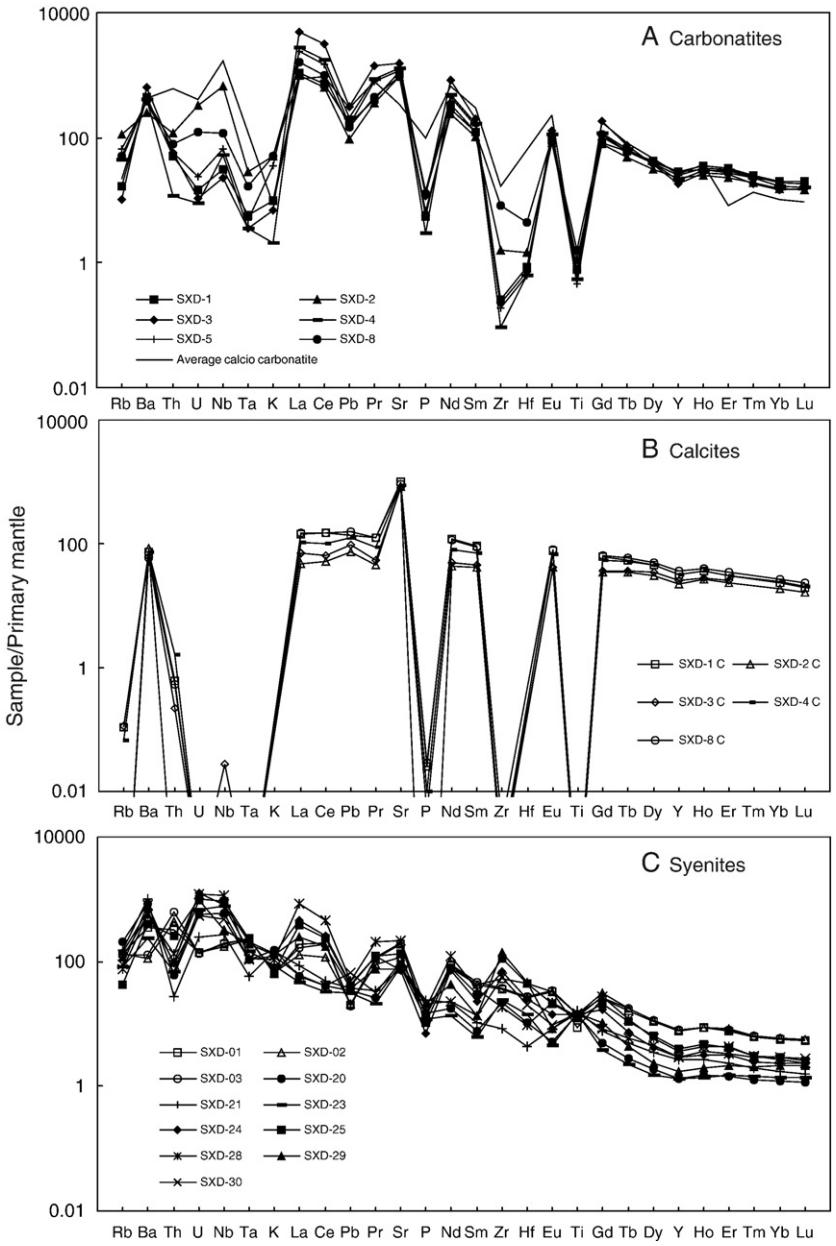

Fig. 4. Primitive mantle-normalized trace-element abundances of carbonatites (A), average calcite cores (B) and syenites (C). In C sample SXD-01, -02 and -03 are fine-grained syenites, and the others are porphyritic syenites. The data for calciocarbonatite are from Woolley and Kempe (1989). Normalized values are from Sun and McDonough (1989).

carbonatite mantle source. The carbonatites are characterized by positive ε_{Nd} (2.5–6) with Nd isotopic model ages (T_{DM}) of 610–840 Ma. Their Sr and Nd isotopes are close to the values expected for HIMU mantle components (Fig. 7). In addition, average calcites show a wide range of $^{207}Pb/^{206}Pb$ (0.785–0.842) and $^{208}Pb/^{206}Pb$ (1.954–2.110) ratios, forming a nearly linear array between EM1 and HIMU (Fig. 8). The contribution of radiogenic Pb is assumed to be negligible given that the calcites contain tens of ppm Pb, and U and Th abundances are below detection limits (Table 3). The syenites have a small range of Sr and Nd isotopic compositions. They are characterized by unradiogenic $(^{87}Sr/^{86}Sr)_0$ of 0.7029–0.7033 and positive ε_{Nd} of 2.8 to 4 with T_{DM} of 730–920 Ma.

5. Discussion

5.1. Genesis of carbonatites

The characteristic Sr abundances and C–O–Sr–Nd–Pb isotopes in the whole rocks and calcite separates support that Shaxiongdong carbonatites are of igneous origin. The rock is spatially associated with the nepheline-bearing alkali-feldspar syenites. They overlap in Sr and Nd isotopic compositions (Fig. 7), which contrasts with data in Harmer and Gitiins (1998) and Srivastava et al. (2005). In their cases carbonatites have obviously different Sr and Nd isotopes from associated silicate rocks. This implies that the Shaxiongdong carbonatites and syenites evolved from the same mantle sources. If the rock types were from the same source, and they were related through partitioning into immiscible silicate–carbonate liquid systems then the experiments by Jones et al. (1995) and Veksler et al. (1998b) should explain many of the observed trace-element patterns, but it does not explain the lack of strong enrichment of Ba in the carbonatites relative to the syenites. Further, the Shaxiongdong carbonatites have anomalously low Th, Nb, P and Zr contents compared to average calciocarbonatites worldwide (Fig. 4A), and all of the HREE can be accounted for by calcite even though the calcite itself has relatively low REE contents and nearly flat chondrite-normalized patterns as noted above (Fig. 5A–E). So two observations

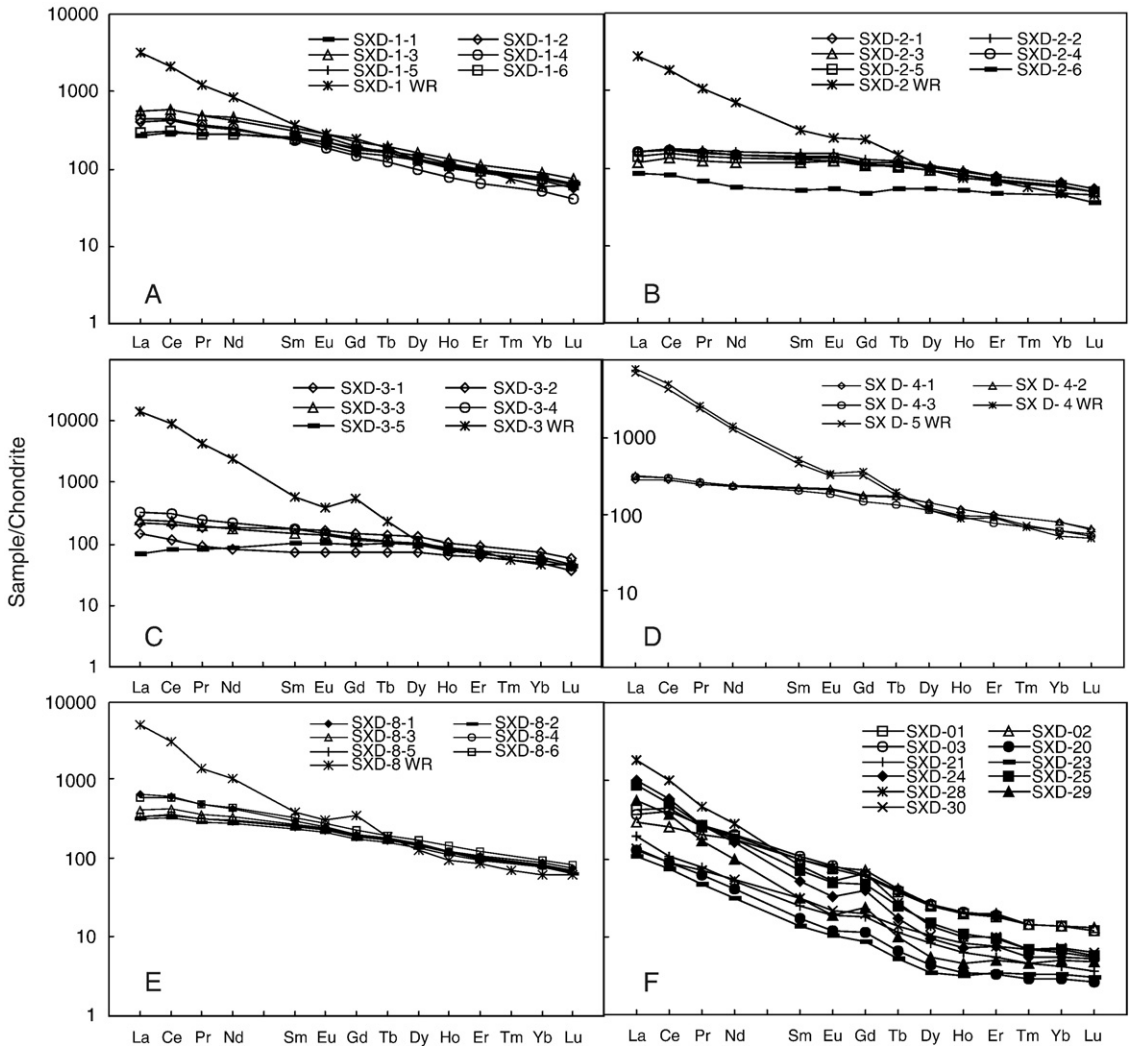

Fig. 5. Chondrite-normalized REE abundances of carbonatites and representative carbonate cores (A–E) and syenites (F). In A–E there are whole rock carbonatite data (WR) plus laser data from calcite from that sample. Symbols for syenites are the same as in Fig. 4. The positive Gd anomaly in some samples is an analytical artifact (see analytical method online). Normalization values are from Sun and McDonough (1989).

need to be explained: the composition of the carbonatite, and the actual composition of the calcite which composes most of the rock. It is difficult to imagine processes other than fractional crystallization whereby trace phases rich in LREE, Nb, P, Zr and Th are removed from the system leaving a calcite cumulate. Given that the Shaxiongdong carbonatites are distinct from carbonates in carbonatites from other localities (e.g. Eby, 1975; Hornig-Kjarsgaard, 1998; Xu et al., 2007) the rocks are good candidates for what Mitchell (2005) calls carbothermal residua. Wyllie and Tuttle (1960) originally showed that calcite cumulates could be produced at

Table 4
C, O, Sr and Nd isotopic data

Samples	SXD-02	SXD-21	SXD-25	SXD-30	SXD-1	SXD-2	SXD-3	SXD-4	SXD-8
Type	FS	PS	PS	PS	C	C	C	C	C
$\delta^{13}C_{PDB}$ (‰)					−6.05	−5.71	−6.08	−5.95	−5.91
$\delta^{18}O_{SMOW}$ (‰)					7.26	8.09	7.57	6.92	8.08
$^{87}Rb/^{86}Sr$	0.077	0.171	0.027	0.077	0.001	0.010	0.001	0.003	0.005
$^{87}Sr/^{86}Sr$ (±2σ)	0.703725±13	0.703961±13	0.703504±12	0.703597±13	0.703177±15	0.703046±53	0.703253±15	0.703082±35	0.703199±18
					0.703194±16		0.703177±17	0.703108±21	0.703191±16
								0.703142±21	
Mean					0.703186	0.703046	0.703215	0.703111	0.703195
$(^{87}Sr/^{86}Sr)_0$	0.70324	0.70289	0.70333	0.70312	0.70318	0.70296	0.70321	0.70309	0.70317
$^{147}Sm/^{144}Nd$	0.110	0.094	0.077	0.113	0.086	0.085	0.047	0.071	0.074
$^{143}Nd/^{144}Nd$ (±2σ)	0.512557±12	0.512534±11	0.512495±15	0.512539±10	0.512448±13	0.512521±13	0.512448±12	0.512575±13	0.512590±14
ε_{Nd} (t)	3.3	3.8	4.0	2.8	2.5	4.0	4.7	5.8	6.0
T_{DM} (Ga)	0.88	0.78	0.73	0.92	0.84	0.75	0.64	0.62	0.61

$^{87}Rb/^{86}Sr$ and $^{147}Sm/^{143}Nd$ ratios are calculated from Rb, Sr, Sm and Nd contents measured by ICPMS (Table 2). Initial Sr and Nd isotopic values are calculated assuming an emplacement age of 440 Ma. ε_{Nd} (t) values are calculated based on present-day $(^{147}Sm/^{143}Nd)_{CHUR}=0.1967$ and $(^{143}Nd/^{144}Nd)_{CHUR}=0.512638$, T_{DM} values based on present-day $(^{147}Sm/^{143}Nd)_{DM}=0.2137$ and $(^{143}Nd/^{144}Nd)_{DM}=0.51315$. Type is the same as in Table 2.

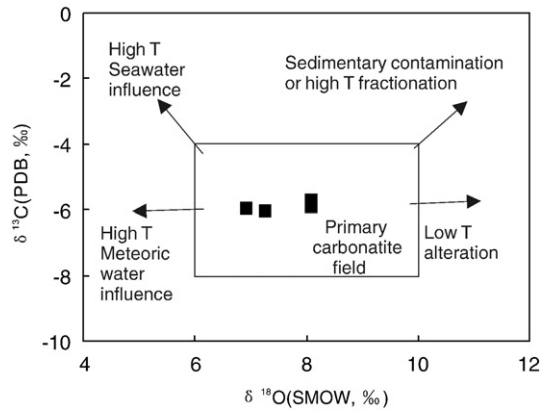

Fig. 6. Carbon and oxygen isotopic compositions of calcites from carbonatites, together with the field of primary, unaltered carbonatites of Keller and Hoefs (1995). Arrows indicate schematically the main processes responsible for changes in the C–O isotopic compositions (Demény et al., 1998).

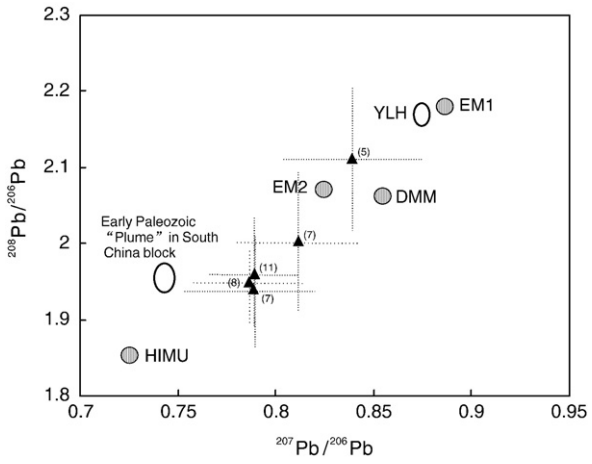

Fig. 8. $^{208}Pb/^{206}Pb$ vs. $^{207}Pb/^{206}Pb$ diagram for average calcite crystals in-situ analyses. The early Paleozoic plume values in South China block are estimated from those of Silurian dyke swarms in Languo (Xu et al., 2001), and Pb isotopes of xenoliths in the dyke swarms are not reported. YLH (Zhang et al., 1997a), DMM, HIMU, EM1, and EM2 (Hart, 1988) are the same as in Fig. 7. The error bars are in-run precision (2σ, standard error).

geologically reasonable temperature (<800 °C) and crustal pressures from a liquid if it contained substantial amounts of H_2O. Therefore, the Shaxiongdong carbonatites may be calcite-rich cumulates, which crystallized from a late-stage fluid derived from a fractioned magma dominated by CO_2 but also containing H_2O, like the carbothermal residua defined by Mitchell (2005).

5.2. Tectonic implications

As summarized by Zhao et al. (1995), alkaline magmas can be generated in almost all tectonic settings, with their tectonic affinities being clearly reflected in their geochemical signatures. They suggested that alkaline syenitic suites formed in subduction-related regimes, or those previously modified by subduction processes, usually showed a characteristic negative Nb anomaly on trace-element distribution spiderdiagram and high Sr isotopic ratios and low ε_{Nb} values, in contrast to trace element and isotope features for those formed in continental rift zones. The nepheline-bearing alkali-feldspar syenites are characterized by negative Pb and no Nb anomalies. They have obviously lower initial Sr isotopes and higher ε_{Nd} values than these synorogen-related granites formed in the Qinling (Fig. 7). Moreover, the carbonatites also show different Sr and Nd isotopes to those emplaced in collision zones (Tilton et al., 1998; Xu et al., 2003), e.g. Northwest Pakistan and West China (Fig. 7). The latter displays high Sr isotopic ratios and low ε_{Nb} values. Importantly, zircon U–Pb age for the syenites is 441 Ma, which is distinctly earlier than the collision of the South China block and South Qinling along the Mianlue suture (200–240 Ma; Li et al., 1996; Sun et al., 2000). This indicates that the complexes formed in a rifting environment, which is further supported by many Ordovician to Silurian alkalic magmatism emplaced in the southern rim of the Qinling (Huang et al., 1992; Ma et al., 2005).

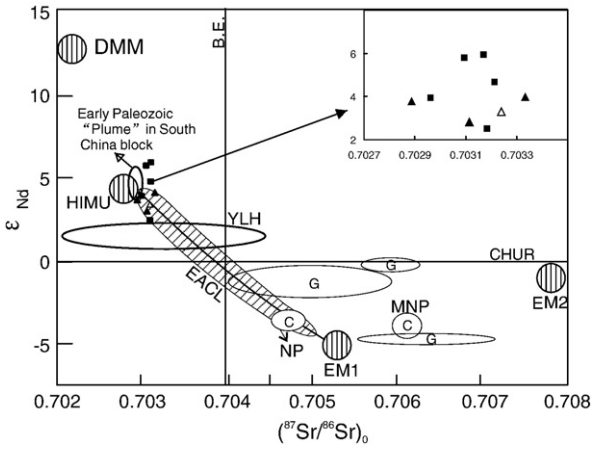

Fig. 7. Sr–Nd isotopic correlation diagram. The early Paleozoic plume values in South China block are estimated from those of xenoliths in Silurian dyke swarms in Languo (Fig. 1) (Lu et al., 2006). YLH, the continental lithosphere values for Shaxiongdong carbonatites are estimated from those of basement of Yaolinghe group (Fig. 1) in the South Qinling (Huang and Wu, 1990). ■, carbonatite; △, ▲, fine-grained and porphyritic syenites, respectively; EACL, East African Carbonatite Line (Bell and Blenkinsop, 1987); NP (C), Northwest Pakistan collision zone carbonatites (Tilton et al., 1998); MNP (C), Himalayan collision zone carbonatites in West China (Xu et al., 2003); G, synorogenic granites in the Qinling (Zhang et al., 1997b; Li et al., 2001; Zhang et al., 2006). DMM, HIMU, EM1 and EM2 are the mantle end-member components (Hart, 1988). Values for lines labelled B.E. (bulk Earth) and CHUR (chondritic uniform reservoir) are those for 440 Ma, assuming present-day values of $^{87}Sr/^{86}Sr_{BE}=0.7045$ and $^{87}Rb/^{86}Sr_{BE}=0.083$ ($\lambda=1.42\times10^{-11}$ per year) and $^{143}Nd/^{144}Nd_{CHUR}=0.512638$ and $^{147}Sm/^{144}Nd_{CHUR}=0.1967$ ($\lambda=6.54\times10^{-12}$ per year).

Silurian ultra-basic and basic dyke swarms (zircon U–Pb and phlogopite ^{39}Ar–^{40}Ar ages from 402 to 432 Ma; Hu et al., 2003; Lu et al., 2006) were emplaced between the South China block and South Qinling (Fig. 1). Although they show a big range of initial Sr isotopic ratios (0.7035–0.7082) and ε_{Nd} (−1.7–4.3) (Xu et al., 2001; Zhao et al., 2003), some of them approximate the compositions of typical HIMU source. The abundance of dike swarms is often cited as evidence for plume activity at that time (Hill, 1993; Li et al., 1999; Guedes et al., 2005). Importantly, some pyroxenite xenoliths were found in these dyke swarms. Based on the geothermometry and geobarometry of pyroxene, Lu et al. (2006) suggested that the magma-derived depth of xenoliths was about 150 km, almost asthenospheric. Their initial Sr isotopic ratios (0.7030–0.7045) and ε_{Nb} (3.7–5.3) (Lu et al., 2006) are also similar to the typical HIMU compositions (Fig. 7). In addition, geodynamicists commonly model anorogenic magmatism as the result of impingement of plume on the lithosphere, with continental rifting as a secondary consequence of lithospheric doming above the plume head (Campbell, 2001; Turcotte and Schubert, 2002). Lithofacies paleogeographic results also show a rapid doming between the South China block and South Qinling at Silurian (Meng and Zhang, 2000). Therefore, plumes may have been active in the South China block during early Paleozoic period but a definitive indicator like a large volume of contemporary continental flood basalt has not been reported in the South China block.

Some researches show that carbonatites forming in a rifting environment track a HIMU and EM1 line in Sr–Nd–Pb isotopic

diagrams, and are related to plume activity (Bell and Simonetti, 1996; Bell and Tilton, 2001). Bell and Simonetti (1996) proposed a two-stage model to explain the HIMU–EM1 signature of carbonatites: (1) release of metasomatizing agents with HIMU signatures from upwelling plume, which in turn metasomatize the sub-continental lithosphere, and (2) variable degrees and discrete partial melting of the resulting heterogeneous, metasomatized lithosphere. The carbonatites and syenites are characterized by negative Pb anomalies (Fig. 4) and low Sr isotopes (Table 4), indicating that they do not contain significant crustal components. Their initial isotopic ratios are inherited from the mantle source region. Fig. 7 supports the significant involvement of HIMU component. Multiple sources may be indicated nonetheless by the fact that the calcites from carbonatites define a trend between HIMU and EM1 on the $^{207}Pb/^{206}Pb$ and $^{208}Pb/^{206}Pb$ diagram (Fig. 8). Thus, a mixing model related the plume can be envisaged in this case. The batholith of Proterozoic Yaolinghe group is an alternative end member, because the calculated T_{DM} for the carbonatites and syenites vary from 610 to 920 Ma, close to the ages of Yaolinghe group (zircon U–Pb ages of 746–808 Ma; Li et al., 2003). They are characterized by low Sr isotopes and positive ε_{Nb} (YLH; Fig. 7). This well explains why the complexes do not show a big variation of Sr and Nd isotopes and fall on the typical HIMU–EM1 mixing line like the East African carbonatites (EACL). The Sr–Nd–Pb isotopic characteristics defined by the complexes may reflect the interaction between upwelling plume and continental lithosphere. The processes resulted in the South Qinling separating from South China block along the Mianlue suture.

6. Conclusions

The following conclusions can be drawn from this work:

1. the emplacement age for Shaxiongdong syenites is 441.8±2.2 Ma and earlier than the collision time between the South China block and South Qinling along the Mianlue suture. The carbonatites and associated nepheline-bearing alkali-feldspar syenites have overlap of Sr and Nd isotopic compositions, suggesting the same mantle sources. Calcites from the carbonatites show low REE contents and flat distribution pattern. This indicates that the rocks may be calcite-rich cumulates from a H_2O-rich liquid derived from intensively fractioned carbonatite magmas.
2. the syenites are characterized by no Nb and negative Pb anomalies. They and associated carbonatites show low initial Sr isotopic ratios and high ε_{Nd}, and approximate the HIMU component. Pb isotopes from the calcites track a HIMU–EM1 mixing line. This indicates that the complexes formed in a rifting environment. The plume activity may be the ultimate cause that controls the early Paleozoic anorogenic magmatism and rifting between the South China block and South Qinling.

Acknowledgments

We thank Prof. M.F. Zhou for supporting trace-element analysis, N. An and L. Kinsley for assistance with the isotopic analytical work, Prof. Z.F. Xue and Dr. M. Wang for prudential petrographic observation. We also thank Prof. X.H. Yu for discussion and two anonymous reviewers for reviewing and improving the manuscript. This research was financially supported by the Chinese '973' Project (No. 2006CB403508) the Chinese National Science Foundation (No. 40773021), and President Scholarship of Chinese Academy of Sciences to C. Xu.

Appendix A. Supplementary data

Supplementary data associated with this article can be found, in the online version, at doi:10.1016/j.lithos.2008.03.002.

References

Ballard, J.R., Palin, J.M., Williams, I.S., Campbell, I.H., 2001. Two ages of porphyry intrusion resolved for the super-giant Chuquicamata copper deposit of northern Chile by ELA-ICP-MS and SHRIMP. Geology 29, 383–386.
Bell, K., Blenkinsop, J., 1987. Nd and Sr isotopic composition of East African carbonatites: implications for mantle heterogeneity. Geology 15, 99–102.
Bell, K., Simonetti, A., 1996. Carbonatite magmatism and plume activity: implications from the Nd, Pb and Sr isotope systematics of Oldoinyo Lengai. Journal of Petrology 37, 1321–1339.
Bell, K., Tilton, G.R., 2001. Nd, Pb, and Sr isotopic compositions of East African cabonatites: evidence for mantle mixing and plume inhomogeneity. Journal of Petrology 42, 1927–1945.
Campbell, I.H., 2001. Identification of ancient mantle plumes. In: Ernst, R.E., Buchan, K.L. (Eds.), Mantle Plumes: Their Identification through Time. Special Paper—Geol. Soc. America, pp. 5–21.
Campbell, I.H., Reiners, P.W., Allen, C.M., Nicolescu, S., Upadhyay, R., 2005. He–Pb double dating of detrital zircons from the Ganges and Indus Rivers: implication for quantifying sediment recycling and provenance studies. Earth and Planetary Science Letters 237, 402–432.
Chakhmouradian, A.R., 2006. High-field-strength elements in carbonatitic rocks: geochemistry, crystal chemistry and significance for constraining the sources of carbonatites. Chemical Geology 235, 138–160.
Demény, A., Ahijado, A., Casillas, R., Vennemann, T.W., 1998. Crustal contamination and fluid/rock interaction in the carbonatites of Fuerteventura Canary Islands, Spain: A C, O, H isotope study. Lithos 44, 101–115.
Eby, G.N., 1975. Abundance and distribution of the rare-earth elements and yttrium in the rocks and minerals of the Oka carbonatite complex, Quebec. Geochimica et Cosmochimica Acta 39, 597–620.
Eggins, S.M., Woodhead, J.D., Kinsley, L.P.J., Mortimer, G.E., Sylvester, P., McCulloch, M.T., Hergt, J.M., Handler, M.R., 1997. A simple method for the precise determination of ≥40 trace elements in geological samples by ICPMS using enriched isotope internal standardization. Chemical Geology 134, 311–326.
Guedes, E., Heilbron, M., Vasconcelos, P.M., Valeriano, C.M., Almeida, J.C.H., Teixeira, W., Filho, A.T., 2005. K–Ar and $^{40}Ar/^{39}Ar$ ages of dikes emplaced in the onshore basement of the Santos Basin, Resende area, SE Brazil: implications for the south Atlantic opening and Tertiary reactivation. Journal of South American Earth Sciences 18, 371–382.
Halama, R., Vennemann, T., Siebel, W., Markl, G., 2005. The GrØnnedal-Ika carbonatite–syenite complex, South Greenland: carbonatite formation by liquid immiscibility. Journal of Petrology 46, 191–217.
Harmer, R.E., Gitiins, J., 1998. The case for primary, mantle-derived carbonatite magma. Journal of Petrology 39, 1895–1903.
Hart, S.R., 1988. Heterogeneous mantle domains: signatures, genesis and mixing chronologies. Earth and Planetary Science Letters 90, 273–296.
Hill, R.I., 1993. Mantle plumes and continental tectonics. Lithos 30, 193–206.
Hornig-Kjarsgaard, I., 1998. Rare earth elements in sovitic carbonatites and their mineral phases. Journal of Petrology 39, 2105–2121.
Hu, J.M., Zhao, G.C., Meng, Q.R., Luo, H., Wang, Z.H., 2003. The geological features and tectonic significances of the basic swarms in Wudang terrain of Qinling orogen. Acta Petrologica Sinica 19, 601–611 (in Chinese with English abstract).
Huang, W.F., 1993. Multiphase deformation and displacement within a basement complex on a continental margin: the Wudang Complex in the Qinling Orogen, China. Tectonophysics 224, 305–326.
Huang, X., Wu, L., 1990. Nd–Sr isotopes of granitoids from Shanxi Province and their significance for tectonic evolution. Acta Petrologica Sinica 2, 1–11 (in Chinese with English abstract).
Huang, Y., Ren, Y., Xia, L., Xia, Z., Zhang, C., 1992. Early Paleozoic bimodal volcanism of northern Dabashan. Acta Petrologica Sinica 8, 253–256 (in Chinese with English abstract).
Ionov, D., Harmer, R.E., 2002. Trace element distribution on calcite–dolomite carbonatites from Spitskop: inferences for differentiation of carbonatite magmas and the origin of carbonates in mantle xenoliths. Earth and Planetary Science Letters 198, 495–510.
Jones, J.H., Walker, D., Picket, D.A., Murrel, M.T., Beate, P., 1995. Experimental investigations of the partitioning of Nb, Mo, Ba, Ce, Pb, Ra, Th, Pa and U between immiscible carbonate and silicate liquids. Geochimica et Cosmochimica Acta 59, 1307–1320.
Keller, J., Hoefs, J., 1995. Stable isotope characteristics of recent natrocarbonatites from Oldoinyo Lengai. In: Bell, K., Keller, J. (Eds.), Carbonatites Volcanism: Oldoinyo Lengai and Petrogenesis of Natrocarbonatites. LAVCEI Proceeding in Volcanology. Springer-Verlag, Berlin, pp. 113–123.
Kjarsgaard, B.A., Hamilton, D.L., 1989. The genesis of carbonatites by immiscibility. In: Bell, K. (Ed.), Carbonatites: Genesis and Evolution. Unwin Hyman, London, pp. 388–404.
Koster van Groos, A.F., Wyllie, P.J., 1963. Experimental data bearing on the role of liquid immiscibility in the genesis of carbonatites. Nature 199, 801–802.
Lee, W.J., Wyllie, P.J., 1994. Experimental data bearing on liquid immiscibility, crystal fractionation, and the origin of calciocarbonatites and natrocarbonatites. International Geology Review 36, 797–819.
Le Maitre, R.W., Bateman, P., Dudek, A., Keller, J., Lameyre, J., Le Bas, M.J., Sabine, P.A., Schmid, R., So, Ørensen, H., Strekeisen, A., Wooley, A.R., Zanettin, B., 1989. A classification of igneous rocks and glossary of terms. Recommendations of the IUGS, Subcommission on the Systematics of Igneous Rocks. Blackwell, Oxford, p. 193.
Li, S., 1991. Geochemistry and petrogenesis of the Shaxiongdong carbonatites, Hubei Province. Geochimica 3, 245–254 (in Chinese with English abstract).

Li, S.G., Sun, W.D., Zhang, G.W., Chen, J., Yang, Y., 1996. Chronology and geochemistry of metavolcanic rocks from Heigouxia Valley in the MianLue tectonic zone, South Qinling: evidence for a Paleozoic oceanic basin and its close time. Science in China (D) 39, 300–310.

Li, Z.X., Li, X.H., Kinny, P.D., Wang, J., 1999. The breakup of Rodinia: did it start with a mantle plume beneath South China? Earth and Planetary Science Letters 173, 171–181.

Li, W.P., Wang, T., Wang, X.X., 2001. Source of Huichizi granitoid complex pluton in northern Qinling, central China: constrained in element and isotopic geochemistry. Earth Science 26, 269–278 (in Chinese with English abstract).

Li, H.K., Lu, S.N., Chen, Z.H., Xiang, Z.Q., Zhou, H.Y., Hao, G.J., 2003. Zircon U–Pb geochronology of rift-type volcanic rocks of the Yaolinghe group in the South Qinling orogen. Geological Bulletin of China 22, 775–781 (in Chinese with English abstract).

Liang, Q., Hu, J., Gregoire, D.C., 2000. Determination of trace elements in granites by inductively coupled plasma mass spectrometry. Talanta 51, 507–513.

Longerich, H.P., Jackson, S.E., Gunter, D., 1996. Laser ablation inductively coupled plasma mass spectrometric transient signal data acquisition and analyze concentration calculation. Journal of Analytical Atomic Spectrometry 11, 899–904.

Lu, F.X., Zhang, B.R., Han, Y.W., Zhong, Z.Q., Ling, W.L., Zhang, H.F., Zheng, J.P., Hou, Q.Y., 2006. The Three-dimensional Lithospheric Chemical Structure in Qinling–Dabie–Sulu Area. Geological Pubilish House, Beijing. (in Chinese).

Ma, C.Q., She, Z.B., Xu, P., Wang, L.Y., 2005. Silurian A-type granitoids in the southern margin of the Tongbai-Dabieshan: evidence from SHRIMP zircon geochronology and geochemistry. Science in China (D) 48, 1134–1145.

Mattauer, M., Matte, Ph., Malavieille, L., Tapponnier, P., Maluski, H., Xu, Z.Q., Lu, Y.L., Tang, Y.Q., 1985. Tectonics of the Qinling Belt: build-up and evolution of eastern Asia. Nature 293, 212–216.

Meng, Q.R., Zhang, G.W., 2000. Geologic framework and tectonic evolution of the Qinling orogen, central China. Tectonophysics 323, 183–196.

Mitchell, R.H., 2005. Carbonatites and carbonatites and carbonatites. The Canadian Mineralogist 43, 2049–2068.

Nelson, D.R., Chivas, A.R., Chappell, B.W., McCulloch, M.T., 1988. Geochemical and isotopic systematics in carbonatites and implications for the evolution of ocean–island sources. Geochimica et Cosmochimica Acta 52, 1–17.

Ratschbacher, L., Hacker, B.R., Calvert, A., Webb, L.E., Grimmer, J.C., McWilliams, M.O., Ireland, T., Dong, S.W., Hu, J.M., 2003. Tectonic of the Qinling (Central China): tectonostratigraphy, geochronology, and deformation history. Tectonophysics 366, 1–53.

Rubatto, D., Gebauer, D., 2000. Use of cathodoluminescence for U–Pb zircon dating by IOM Microprobe: some examples from the western Alps. In: Pagel, M., Barbin, V., Blanc, P., Ohnenstetter, D. (Eds.), Cathodoluminescence in Geoscience. Springer-Verlag, Berlin Heidelberg, Germany, pp. 373–400.

Srivastava, R.K., Sinha, A.K., 2004. The early Cretaceous Sung Valley ultramafic–alkaline–carbonatite complex, Shillong Plateau, northeastern India: petrological and genetic significance. Mineralogy and Petrology 80, 241–263.

Srivastava, R.K., Heaman, L.M., Sinha, A.K., Sun, S.H., 2005. Emplacement age and isotope geochemistry of Sung Valley alkaline–carbonatite complex, Shillong Plateau, northeastern India: implications for primary carbonate melt and genesis of the associated silicate rocks. Lithos 81, 33–54.

Sun, S.S., McDonough, W.F., 1989. Chemical and isotopic systematics of oceanic basalt: implications for mantle compositions and processes. In: Saunders, A.D., Norry, M.J. (Eds.), Magmatism in the Ocean Basins. The Geological Society Special Publication, vol. 42, pp. 313–345.

Sun, W.D., Li, S.G., Chen, Y.D., Li, Y.J., 2000. Zircon U–Pb dating of granitoids from South Qinling, Central China and their geological significance. Geochimica 29, 209–216 (in Chinese with English abstract).

Sun, W.D., Li, S.G., Sun, Y., Zhang, G.W., Li, Q.L., 2002. Mid-paleozoic collision in the north Qinling: Sm–Nd, Rb–Sr and $^{40}Ar/^{39}Ar$ ages and their tectonic implications. Journal of Asian Earth Sciences 21, 69–76.

Sweeney, R.J., 1994. Carbonatite melt compositions in the Earth's mantle. Earth and Planetary Science Letters 128, 259–270.

Tilton, G.R., Bryce, J.G., Mateen, A., 1998. Pb–Sr–Nd isotope data from 30 and 300 Ma collision zone carbonatites in Northwest Pakistan. Journal of Petrology 39, 1865–1874.

Treiman, A.H., 1989. Carbonatites magma: properties and processes. In: Bell, K. (Ed.), Carbonatites: Genesis and Evolution. Unwin Hyman, London, pp. 89–104.

Turcotte, D.L., Schubert, G., 2002. Geodynamics. Cambridge University Press, Cambridge.

Veksler, I.V., Nielsen, T.F.D., Sokolov, S.V., 1998a. Mineralogy of crystallized melt inclusions from Gardiner and Kovdor ultramafic alkaline complexes: implications for carbonatite genesis. Journal of Petrology 39, 2015–2031.

Veksler, I.V., Petibon, C., Jenner, G.A., Dorfman, A.M., Dingwell, D.B., 1998b. Trace element partitioning in immiscibility and silicate liquid: an initial experimental study using a centrifuge autoclave. Journal of Petrology 39, 2095–2104.

Wang, T., Yan, F.M., 1989. Burbankite in carbonatites from Huibei Province. Acta Mineralogica Sinica 9, 345–351 (in Chinese with English abstract).

Williams, R.W., Gill, J.B., Bruland, K.W., 1986. Ra–Th disequilibria systematics: timescale of carbonatites magma formation at Oldoinyo Lengai volcano, Tanzania. Geochimica et Cosmochimica Acta 50, 1249–1259.

Woodhead, J.D., Hergt, J.M., 2000. Pb-isotope analyses of USGS reference materials. Geostandards 24, 33–38.

Woolley, A.R., Kempe, D.R.C., 1989. Carbonatites: nomenclature, average chemical composition. In: Bell, K. (Ed.), Carbonatites: Genesis and Evolution. Unwin Hyman, London, pp. 1–14.

Wyllie, P.J., Tuttle, O.F., 1960. The system $CaO–CO_2–H_2O$ and the origin of carbonatites. Journal of Petrology 1, 1–46.

Xu, X.Y., Xia, L.Q., Xia, Z.C., Huang, Y.H., 2001. Geochemical characteristics and petrogenesis of the early Paleozoic alkali lamprophyre complex from Langao County. Acta Geoscientia Sinica 22, 55–60 (in Chinese with English abstract).

Xu, C., Huang, Z.L., Liu, C.Q., Qi, L., Li, W.B., Guan, T., 2003. Geochemistry of carbonatites in Maoniuping REE deposit, Sichuan Province, China. Science in China (D) 46, 246–256.

Xu, C., Campbell, I.H., Allen, C.M., Huang, Z.L., Qi, L., Zhang, H., Zhang, G.S., 2007. Flat rare earth element patterns as an indicator of cumulate processes in the Lesser Qinling carbonatites, China. Lithos 95, 267–278.

Xue, F., Lerch, M.F., Kroner, A., Reischmann, T., 1996. Tectonic evolution of the East Qinling Mountains, China, in the Paleozoic: a review and new tectonic model. Tectonophysics 253, 271–284.

Zhang, H.F., Gao, S., Zhang, B.R., Luo, T.C., Lin, W.L., 1997a. Pb isotopes of granitoids suggest Devonian accretion of Yangtze (south China) craton to north China craton. Geology 25, 1015–1018.

Zhang, H.F., Ouyang, J.P., Lin, W.L., Chen, Y.L., 1997b. Pb, Sr, Nd isotope compositions of Ningshan granitoids, south Qinling and their deep geological information. Acta Petrologica et Mineralogica 16, 22–32 (in Chinese with English abstract).

Zhang, H.F., Zhang, B.R., Harris, N., Zhang, L., Chen, Y.L., Chen, N.S., Zhao, Z.D., 2006. U–Pb zircon SHRIMP ages, geochemical and Sr–Nd–Pb isotopic composition of intrusive rocks from the Longshan–Tianshui area in the southeast corner of the Qilian orogenic belt, China: constraints on petrogenesis and tectonic affinity. Journal of Asian Earth Sciences 27, 751–764.

Zhao, J.X., Shiraishi, K., Ellis, D.J., Sheraton, J.W., 1995. Geochemical and isotopic studies of syenites from the Yamato Mountains, East Antarctica: implications for the origin of syenitic magmas. Geochimica et Cosmochimica Acta 59, 1363–1382.

Zhao, G.C., Hu, J.M., Meng, Q.R., 2003. Geochemistry of the basic sills in the western Wudang block: the evidences of the Paleozoic underplating in the south Qinling. Acta Petrologica Sinica 19, 612–622 (in Chinese with English abstract).